Int. J. Multiphase Flow Vol. 11, No. 6, pp. 741–760, 1985
Printed in Great Britain.

0301-9322/85 $3.00 + .00

FLOODING IN VERTICAL TWO-PHASE FLOW

K. W. McQUILLAN†, P. B. WHALLEY
Department of Engineering Science, University of Oxford, Oxford OX1 3PJ, England

and

G. F. HEWITT
Engineering Sciences Division, AERE Harwell, England

(*Received* 12 *November* 1984; *in revised form* 18 *March* 1985)

Abstract—The phenomenon of flooding limits the stability of a liquid film falling along the walls of a tube in which a gas is flowing upward. This paper describes a series of experiments to observe and photograph the flooding process. Flooding in a vertical perspex tube was observed by viewing axially along the tube from the top, and flooding on the walls of a stainless steel rod supported centrally within a perspex tube was observed by viewing normally through the tube walls. The resulting observations show that flooding occurs as a result of the formation and motion of a large disturbance wave on the surface of the liquid film. A simple theoretical treatment of flooding is presented, based on the observations of the flooding disturbance. The resulting equations enable the calculation of the gas velocity and the liquid wave height at flooding, and the predictions are in good agreement with experimental observations reported here and elsewhere.

1. INTRODUCTION

If a liquid film is introduced uniformly around the periphery of a vertical tube it flows downwards along the walls of the tube under the influence of gravity. The liquid film is not smooth, but has small ripples on its surface. The liquid film flow is however stable, the ripples do not grow very large, and the liquid film can be removed at the bottom of the tube. If now a gas is introduced at the bottom of the tube and its flowrate slowly increases from zero, the falling liquid film continues to exist but becomes progressively more disturbed until, at some critical value of the gas flowrate, some of the liquid moves upward along the tube, eventually climbing above its point of injection. The phenomenon which causes this transition is called flooding.

Flooding is of importance in both the power and process industries, and consequently has been widely studied with the aim of providing methods by which flooding conditions may be calculated. As a result of this research there are a large number of correlating equations at the disposal of the engineer who wishes to predict the flooding gas velocity in a given situation. These correlations are of two main types. The first group are based largely on experimental flooding data, often supplemented by dimensional analysis. This type of empirical flooding correlation must be used carefully, particularly when predictions are required for conditions or fluids other than those for which the correlation was developed. The second group of equations are based on physical and mathematical modelling of the flooding event, and should therefore be more widely applicable. However, the complicated nature of flooding has resulted in several different mechanisms being postulated as its cause, and this uncertainty has limited the success of the available theoretical flooding treatments. Whalley & McQuillan (1985) have reviewed the possible flooding mechanisms, and have performed experiments to investigate the postulation that flooding occurs as a result of wave growth on the falling liquid film.

This paper describes two experiments in which flooding was observed, both visually and with the aid of high-speed cine photography, in an attempt to gain detailed information about the formation and motion of the flooding disturbance, and hence about the mechanism

†Present address: ICI Agricultural Division, Billingham, Cleveland, England.

by which flooding occurs. Several investigations have been made to observe flooding by viewing the flow normally through the walls of a transparent tube, and there is good agreement concerning the sequence and description of the events by which flooding occurs; see for example Whalley & McQuillan (1985). However, viewing the flow normally through the tube wall can only yield limited information about the exact nature of the flooding disturbance, because the light leaving the tube undergoes a complex series of refractions in passing through the liquid film and the tube wall. The experiments described in this report overcame this problem as follows:

1. In the first series of experiments flooding in a vertical tube was observed by viewing axially along the tube.
2. In the second series of experiments the liquid film flowed along the walls of a vertical stainless steel rod, and the gas flowed in the annular gap between the rod and a perspex tube. Flooding was observed by viewing normally through the walls of the perspex tube.

2. OBSERVATION OF FLOODING BY AXIAL VIEW PHOTOGRAPHY

All observations were made with air and water flowing in perspex tube of inside diameter 0.032 m. Two types of experiment were performed:

1. Flooding was induced by lowering the pressure in the test section, hence increasing the gas velocity. This technique was chosen because flooding may be induced by small reductions in pressure (of approximately 0.05 bar).
2. Flooding was induced by the injection of artificial waves into the falling water film using the method described by Whalley & McQuillan (1985).

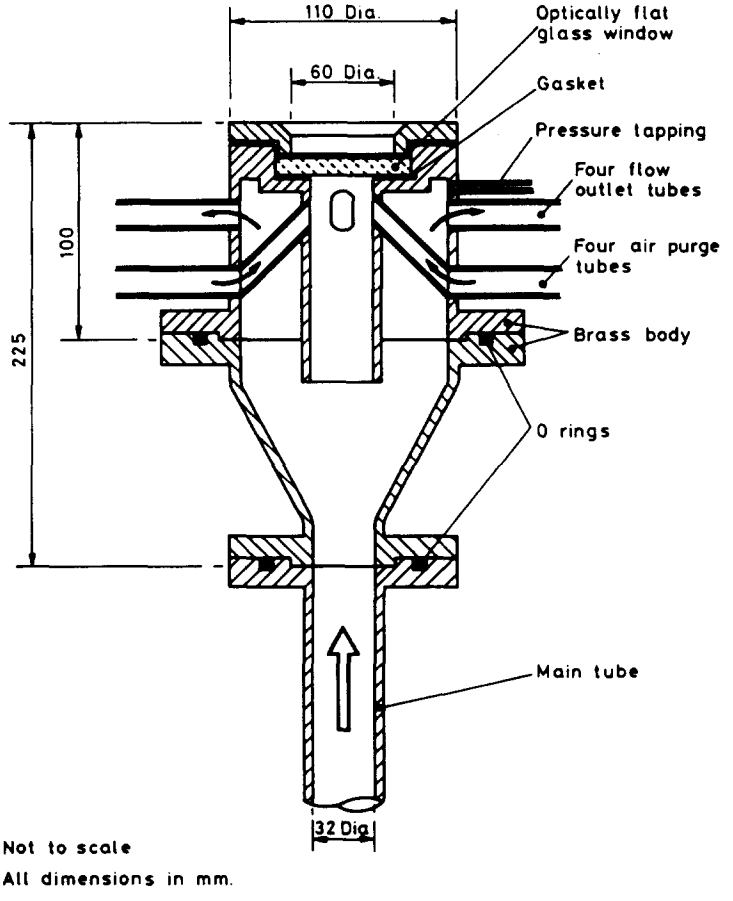

Figure 1. Axial flow viewing section.

The axial flow viewing section is shown in figure 1, and its development and use has been described fully by Hewitt & Whalley (1980). For the observation of flooding it was found sufficient to use the air purge system intermittently, to remove droplets from the viewing window after each flooding observation. This was possible because, in the unflooded flow, the water did not reach either viewing window.

Figure 2 shows the basic layout of the apparatus. Air was introduced through the bottom viewing section and flowed alone in the tube for a calming length of 0.5 m. The water film was introduced through a sinter section situated immediately below the top viewing section. The sinter section for wave injection was positioned below the water film inlet sinter. The water film and injected waves then flowed along the walls of the test section before being removed at a sinter section situated 1.0 m below the wave injection sinter section.

Figure 3 shows the layout of the photographic equipment. The walls of the tube were coloured as shown in figures 2 and 3, using "Letraset" colour overlay. The use of colour film for the photographic runs then enabled the approximate axial position of disturbances or droplets to be determined. The test section was lit from the bottom using a standard 300 W slide projector with a diffuser between the projector and the bottom viewing window, and side light was provided by eight 1 kW lamps.

2.1. *Axial view experiments*

The axial view experiments were conducted with a water film flowrate of 63.0 g/s and at a pressure of approximately 1.5 bar. Air was introduced to the rig and allowed to leave by both the main air outlet and the water film removal sinter. The falling water film was then established and the valve on the water film removal sinter adjusted to enable all of the water film to be removed from the rig, accompanied by as little air as possible (see Whalley & McQuillan 1985). The air flowrate was then increased to a value slightly below the flooding air flowrate, whilst maintaining the pressure at 1.5 bar using the valve on the main air outlet. The flow was then left for a few minutes to ensure its stability. Flooding was then induced and recorded photographed at 500 frames/s. This speed was chosen as a compromise

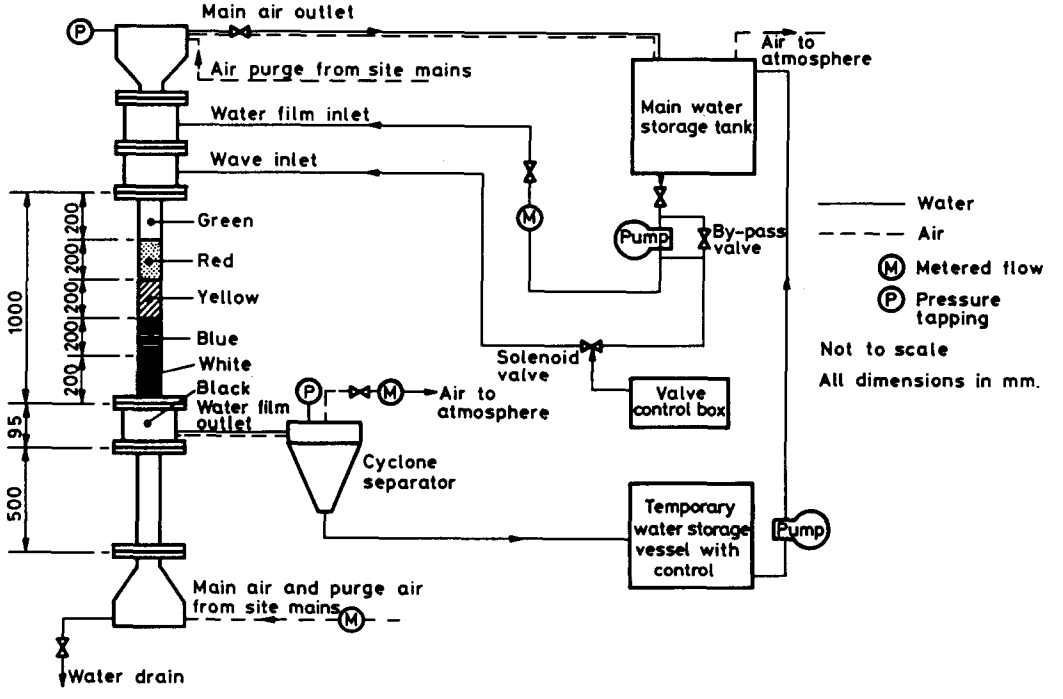

Figure 2. Experimental arrangement for observation of flooding by axial view photography.

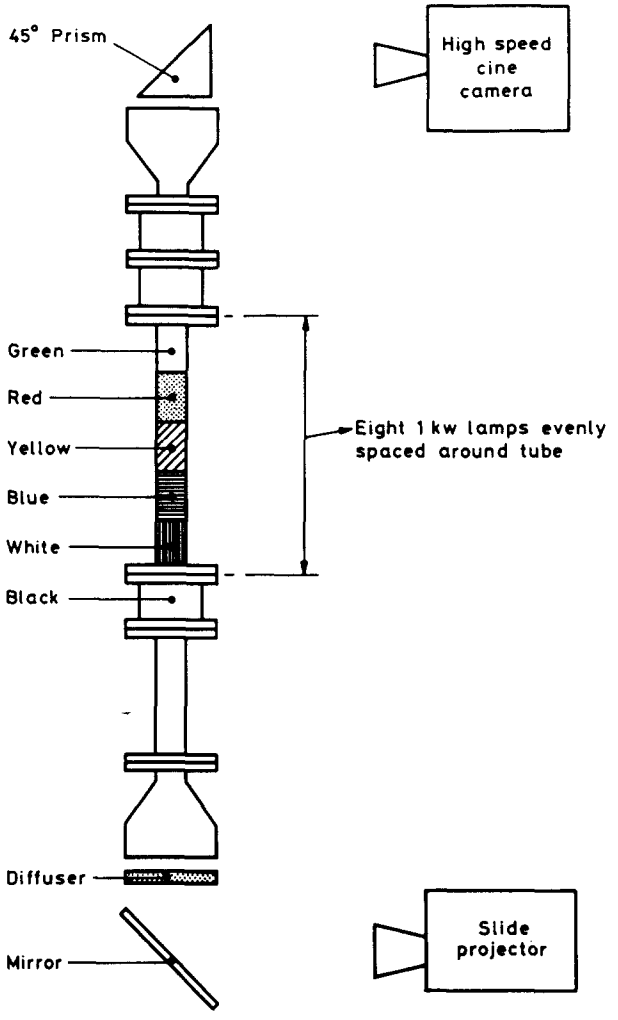

Figure 3. Photographic arrangement for observation of flooding by axial view photography.

between the conflicting requirements of:

(i) high speed to give a slow motion view of the events, and
(ii) low speed to give a reasonably long running time and to enable a small aperture to be used, thus giving a large depth of field.

Flooding was induced in the following two ways:

1. Filming was commenced and 1 s allowed for the camera to reach the correct speed. The rig pressure was then gradually reduced by opening the air outlet valve. Providing that the initial air flowrate was greater than approximately 98% of the flooding air flowrate, flooding could be induced by a drop in pressure of less than 0.05 bar.
2. After starting filming artificial waves were injected into the flow, either singly or at a given frequency. Each injected wave contained 4 ml of water.

2.2. *Axial view results*

2.2.1. *Flooding by lowering rig pressure.* Figure 4 gives schematic representations of the form and motion of the flooding disturbance. This method of presenting the information was chosen because of the poor quality of still photographs taken from cine films. When studying

figure 4 the following should be noted:

1. The filming technique produced a normal perspective view of the tube, and therefore the bottom of the test section appeared to be smaller in diameter than the top. As a consequence of this, a smooth film could be identified by the observation of a number of concentric coloured rings, with the rings near the top of the rig being larger than those near the bottom. For the sake of clarity figure 4 has been drawn under the assumption that for a smooth film the coloured rings would be of equal size, and therefore disturbances may be recognised by inequalities in ring widths or by the blocking of some of the rings.
2. Loss of focus meant that the green ring could not be observed.
3. The part of the flow coloured black was in the water film outlet sinter, where the side lighting was unable to penetrate.
4. The hatching is such that there is an increase in hatching density in moving from the top to the bottom of the tube.
5. The time given below each view of the flow is measured from an arbitrary zero; it is not the time after flooding was initiated.

Figure 4 illustrates the types of flow observed before and during the flooding event, and a description of each flow is given below.

1. In figure 4a the air velocity is slightly below the flooding air velocity. The falling water film is highly disturbed, particularly in the blue and white regions and in the water

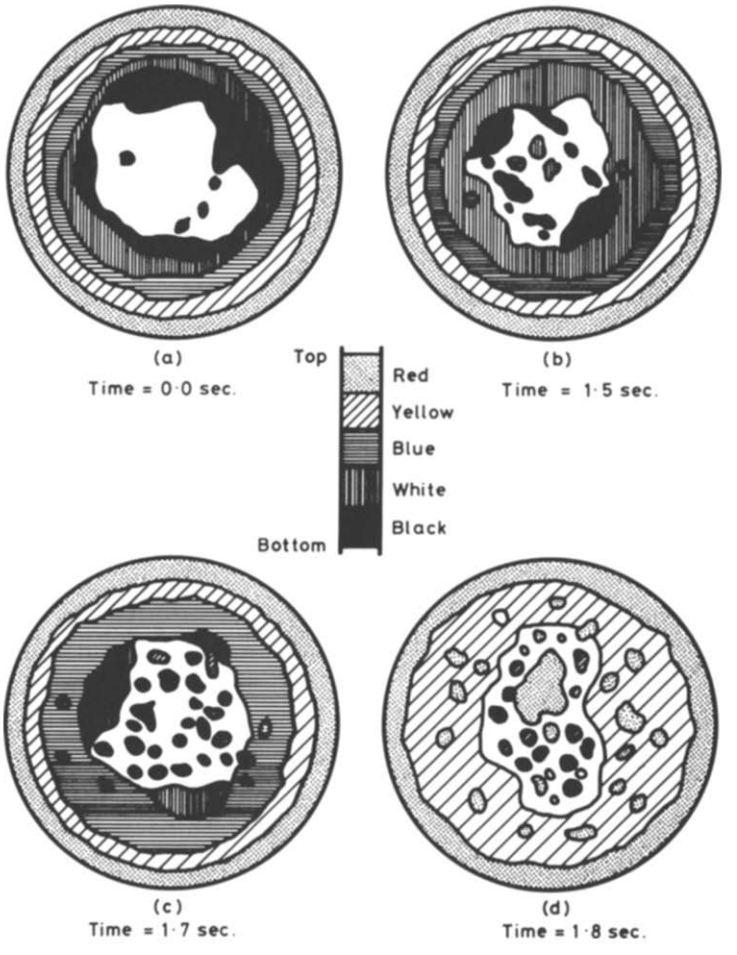

Figure 4. Schematic representation of flooding by lowering rig pressure.

outlet sinter (black). On some films it was possible to observe a wavelike disturbance growing as it moved downward along the walls of the tube. There is a small amount of water entrainment in figure 4a, but none of the entrained droplets move upwards in the air flow.

2. In figure 4b the pressure has been reduced and consequently the air velocity has increased slightly, reaching the value at which flooding occurs. In all of the films in which the pressure was reduced the flooding event began with the sudden formation of a large disturbance, either in the white section of tube or in the water film removal sinter. The disturbed region was continuous around the wall of the tube, and its amplitude varied between approximately 5 and 10 mm.

3. In figure 4c the disturbed region of water film has moved upward along the tube and become predominantly blue. The number of entrained water droplets has increased from almost zero at the initial formation of the disturbance, and some of the entrained droplets are coloured yellow and losing focus slightly. This indicates that the flooding disturbance is the source of entrainment, with droplets being ripped from its peak and then traveling along the tube ahead of the disturbance.

4. In figure 4d there has been a further increase in the number of entrained droplets, some of which are now red. The flooding disturbance has continued to travel along the tube, but both droplets and disturbance have become blurred due to photographic limitations.

2.2.2. *Flooding by artificial wave injection.* The effect of artificial wave injection was found to be extremely sensitive to the pressure in the test section, and is described fully by Whalley & McQuillan (1984). For the purposes of this paper it is sufficient to note that under some circumstances artificially injected waves could be observed to fall along the walls of the tube, and in so doing appear to grow and to cause a flooding disturbance indistinguishable from that occurring as a result of lowering the pressure in the test section.

3. OBSERVATION OF FLOODING IN AN ANNULUS

The use of axial view photography to observe flooding has enabled the growth and motion of the flooding disturbance to be studied. In order to obtain a more detailed observation of the growth of the flooding disturbance it was necessary to view the flow normally (from the side), because in the axial view experiments the flooding disturbance was inevitably created some distance from the camera. This section describes an experiment designed to enable the normal observation of flooding on the walls of a vertical stainless steel rod supported centrally within a perspex tube.

3.1. *Annulus apparatus*

The general layout of the apparatus is shown in figure 5. The falling water film was introduced around the outer wall of the central tube through a short section of tube wall made from sintered bronze, and removed through a similar sinter section situated 0.3 m below the first. Air was introduced through the four inlet tubes in the brass bottom section. The air then flowed upward along the annular gap between the central tube and the three perspex sections before being removed through the single outlet tube in the top brass section. The various sections of the apparatus are described individually below.

3.1.1. *Central tube.* The central tube was made of 38 mm outside diameter stainless steel tube with a wall thickness of 9 mm.

3.1.2. *Water film inlet and outlet sinter sections.* The assembly of the water film inlet and outlet sinter sections is illustrated in figure 6. Care was taken to ensure a smooth transition between the stainless steel and the bronze on the surface of the central tube. This reduced the tendency for droplets of water to be entrained into the air stream, particularly at the top of the outlet sinter section.

3.1.3. *Brass bottom and top sections.* The brass bottom and top sections are illustrated in figure 5. The use of four inlet tubes for the air ensured an even distribution of the air at the

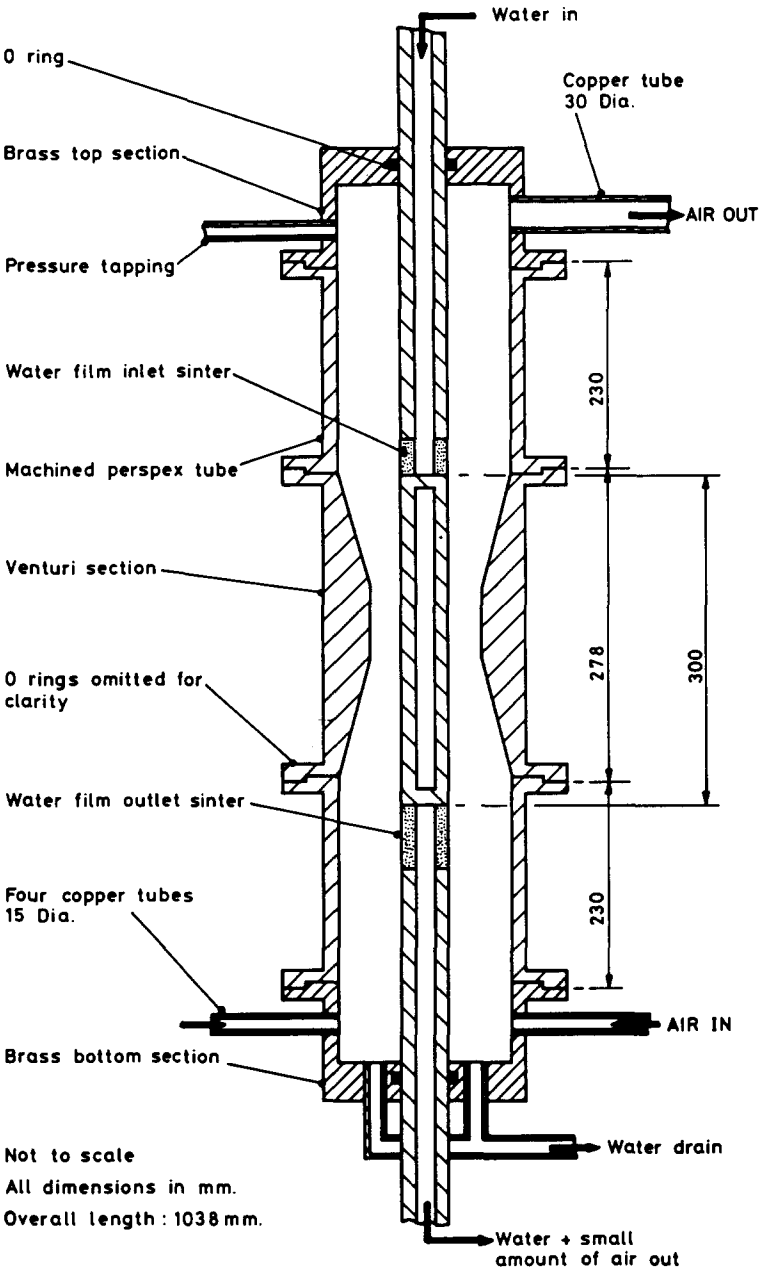

Figure 5. Experimental arrangement for observation of flooding in an annulus.

inlet. Two drain holes in the bottom face enabled the system to be periodically drained of accumulated water. The top section had a single large diameter air outlet tube and a pressure tapping.

3.1.4. *Perspex sections.* The perspex venturi section is illustrated in figure 7. The flow area at the throat of the venturi was 43% of the flow area at the outlet sinter. The use of a venturi section caused the gas velocity to vary along the length of the annulus. Flooding was expected to occur in the region of the rod over which the gas velocity had its maximum value. The use of a venturi therefore served two purposes:

1. It enabled the position of formation of the flooding disturbance to be predicted. It was therefore sufficient to observe a small section of the tube wall with the camera and hence obtain a large magnification.

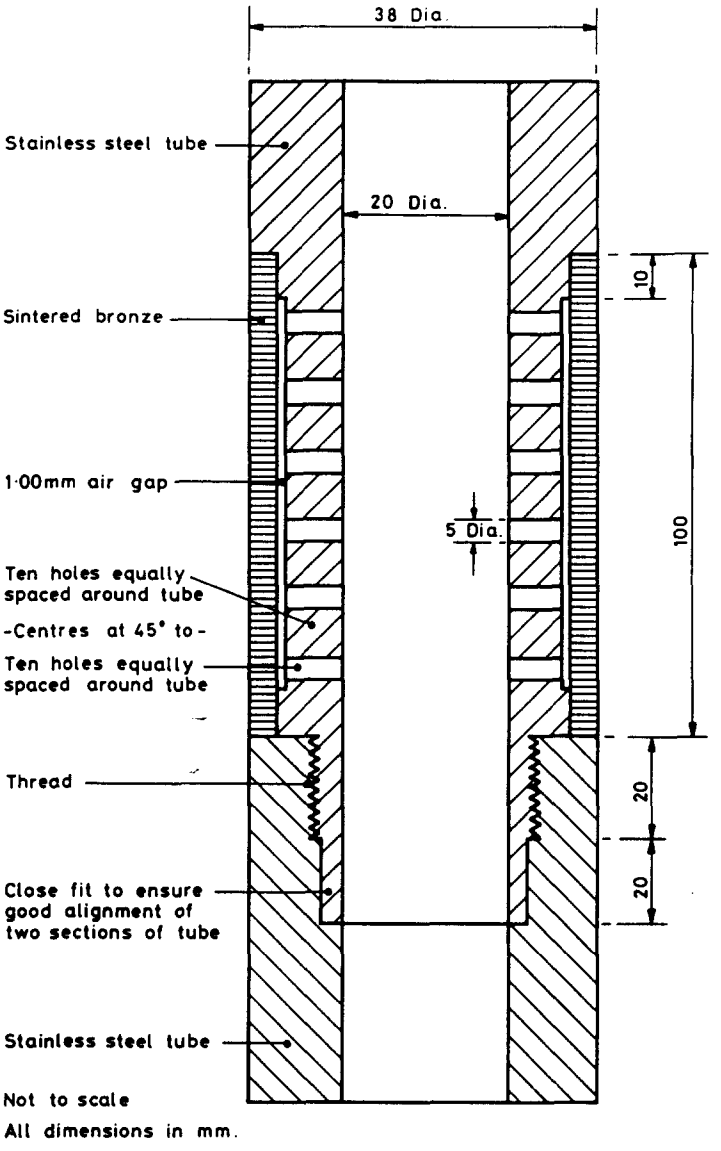

Figure 6. Section through stainless steel tube illustrating the water film removal sinter section.

2. It enabled flooding to occur at a position remote from the outlet sinter, thereby removing end effects.

The perspex tube sections are illustrated in figure 5. The inner walls of these sections were machined to the required diameter to ensure that there were no steps in diameter at the flanges.

The photographic system was set to provide a normal view of the part of the stainless steel rod contained within the venturi throat. Four 1 kW lamps provided frontal lighting, and diffused back lighting enabled the profile of the falling liquid film to be observed. The use of black and white film, together with smaller depth of field and lower lighting intensity requirements enabled the filming rate to be increased from 500 frames/s in the axial view experiments to 1000 frames/s.

3.2. *Annulus experiments*

The experiments to observe flooding in an annulus were performed with a water film flowrate of 63.0 g/s and at a pressure of approximately 1.5 bar as in the axial view

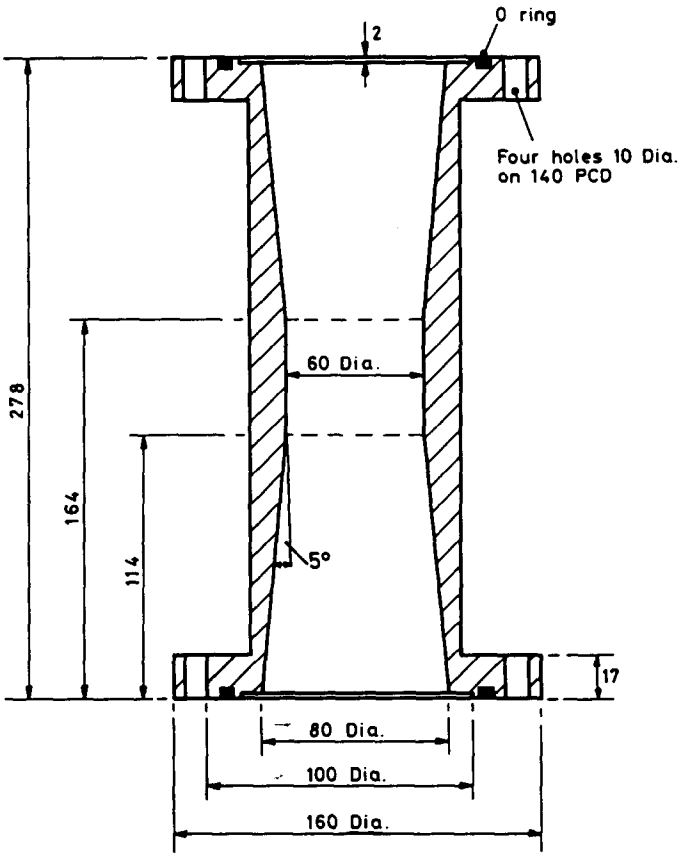

Figure 7. Perspex venturi section.

experiments. Air was introduced to the rig and allowed to leave via the main air outlet and the water film removal sinter. The falling water film was then established and the air flowrate increased to a value slightly below the flooding air flowrate. Flooding was then induced by lowering the rig pressure and simultaneously increasing the air flowrate. In a separate series of experiments flooding air flowrates were measured for 10 water film flowrates at a pressure of 1.5 bar. The air removed at the water film removal sinter was subtracted from the total air flow as described by Whalley & McQuillan (1985).

3.3. *Annulus results*

The measured flooding air and water flowrates are shown in figure 8. The flooding air velocity decreases as the water film flowrate increases.

Figure 9 presents a selection of frames from the cine films of flooding in an annulus. The following points should be noted:

1. Some of the information present on the cine films is lost in figure 9.
2. The time given below each view of the flow is measured from an arbitrary zero.
3. The lighting was concentrated on the left hand side of the central tube.

Figure 9 shows the falling liquid film at a point when the gas velocity is such that flooding is about to occur. In figure 9(a)–(o) a series of waves are formed on the surface of the falling film at a point just below the top of the venturi throat. The waves were first observed at lower gas flowrates. As the waves travel along the surface of the water film they increase in

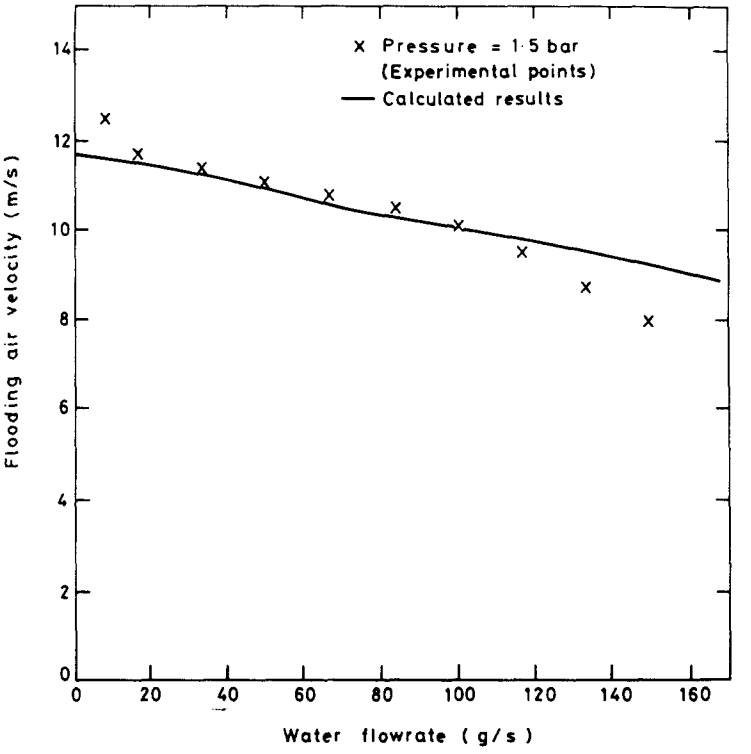

Figure 8. Experimental and predicted flooding velocities for flow in the annulus.

amplitude and also slow down (and hence their separation decreases). It was noticeable that at low gas flowrates the waves were not continuous around the walls of the central tube, but that as the gas flowrate increased the waves spread around the walls, eventually becoming continuous.

In figure 9(e) a wave has become stationary at a point tube slightly below the bottom of the venturi throat, and remains approximately stationary in figures 9(e)–(j). The stationary wave is joined by other waves falling along the surface of the central tube [noticeable here in figures 9(i) and 9(j)] and hence its amplitude increases. Occasional droplets are entrained from the surface of the wave in figures 9(i)–(j) and these droplets move predominantly upwards in the gas flow. In figure 9(k) there is an increase in the amount of entrainment and the stationary wave begins to move upward along the tube wall (approximately 0.1 s after becoming stationary). This upwards motion continues in figures 9(l)–(o) and leads to flooding.

4. THE MECHANISM BY WHICH FLOODING OCCURS

An axial view photographic technique has been used to observe the formation and motion of the flooding disturbance, and colouring of the test section wall has enabled the axial motion of the flooding disturbance to be tracked. The resulting high-speed cine films have enabled the following conclusions to be made:

1. On increasing the air flowrate flooding occurs by the sudden formation of a wavelike disturbance at or near the water film outlet, and by the subsequent upward motion of the disturbance wave along the tube.

2. There is little droplet entrainment and no upward motion of droplets prior to the formation of the flooding disturbance. Water droplets are entrained from the tip of the flooding disturbance and travel up the tube ahead of the main disturbance.

3. For air flowrates slightly below the flooding air flowrate artificially injected waves grow to form a disturbance indistinguishable from the flooding disturbance.

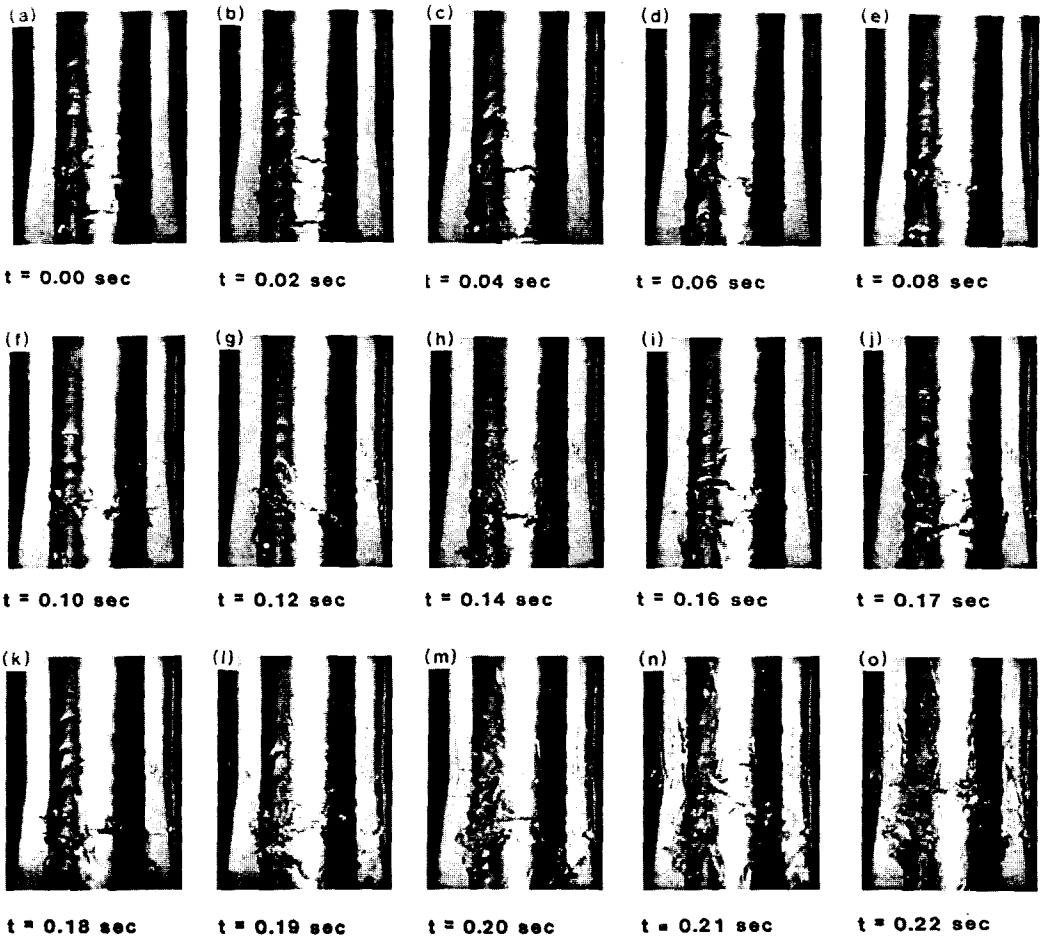

Figure 9. A selection of frames from the high speed cine films of flooding in the annulus. Water flowrate = 70 g/s.

A normal photographic technique has been used to observe flooding on the surface of a stainless steel rod supported centrally within a perspex tube. The resulting high speed cine films have enabled the following additional conclusions to be made:

4. The observations confirm the importance of wave growth, as postulated by Whalley & McQuillan (1985), in the flooding process. The sequence of events immediately before flooding seems to be:

(i) As the gas flowrate is increased waves are formed on the surface of the liquid film.

(ii) These waves increase in amplitude as they travel downward.

(iii) The velocity of the falling waves decreases as they fall until eventually a liquid wave becomes stationary at the bottom of the test section.

(iv) The stationary wave grows and becomes the source of liquid entrainment. The entrained droplets, and eventually the wave, move upward to cause flooding (see (2) above).

5. A SIMPLE ANALYSIS OF FLOODING

Observations have shown that for gas velocities lower than the flooding gas velocity the liquid wave falls along the walls of the tube, but that its velocity decreases as the gas velocity increases until, at the flooding gas velocity, the falling wave becomes stationary for a short time (approximately 0.1 s) and then begins to move vertically upward to cause flooding.

The wave behaviour described above suggests that flooding could be modelled by calculation of the conditions under which the weight of a falling liquid wave is balanced by the forces tending to cause the wave to move upward along the tube walls. None of the available theoretical treatments of flooding described provides such an analysis, although Richter (1981) calculates a critical film thickness from an approximate force balance on a wave.

It may be noted that Shearer & Davidson (1965) have performed an analysis which relates the amplitude of a stationary wave formed on a falling liquid film to the countercurrent gas velocity. Their analysis predicted that the amplitude of the stationary wave becomes large for some value of the gas velocity. Shearer & Davidson (1965) used their analysis to predict flooding conditions by assuming that stationary liquid waves exist on liquid films close to flooding, and that flooding occurs when the gas velocity becomes sufficient to make the amplitude of such waves large. This suggested flooding mechanism is not consistent with the events observed in section 3 above, where stationary waves do not exist until the gas velocity reaches that at which flooding occurs.

The analysis which follows is based on the model of flooding illustrated in figure 10. A wave, of semicircular profile and amplitude h, is assumed to be present on the falling liquid film. Flooding is assumed to occur when the forces on the wave are such that the wave is in equilibrium in both the horizontal and vertical directions. The analysis is performed for flow on the inner walls of a vertical tube. Slightly different equations result if the liquid is flowing

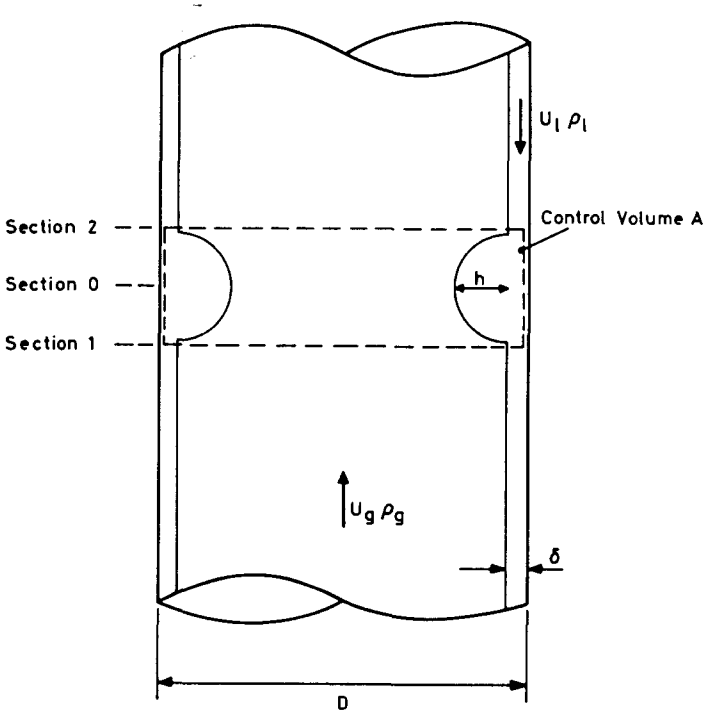

D = Tube inside diameter (m)
h = Wave amplitude (m)
U_g = Gas velocity (m/s)
U_l = Liquid velocity (m/s)
δ = Mean liquid film thickness (m)
ρ_g = Gas density (Kg/m^3)
ρ_l = Liquid density (Kg/m^3)

Figure 10. Model used in theoretical treatment of flooding.

along the outer walls of a vertical rod and the gas in the annular gap between the rod and a vertical tube. The necessary modifications are given below.

In order to determine the forces acting on the liquid wave it is necessary to calculate the pressure difference ΔP where

$$\Delta P = P_1 - P_2, \qquad [1]$$

where P_1 = pressure at section 1, see figure 10 (N/m^2),
P_2 = pressure at section 2, see figure 10 (N/m^2).

The pressure difference between sections 1 and zero may be calculated by the application of Bernoulli's theorem (neglecting changes in the gas static pressure).

$$P_1 - P_0 = \frac{1}{2}\rho_G U_G^2 \left[\left(\frac{A_1}{A_0}\right)^2 - 1\right], \qquad [2]$$

where A_0 = cross-sectional area available for gas at section 0 ($=0.25\pi[D - 2 \cdot (h + \delta)]^2$ m^2),
A_1 = cross-sectional area available for gas at section 1 ($=0.25\pi(D - 2\delta)^2$ m^2),
P_0 = pressure at section 0 (N/m^2),
U_G = gas average velocity at sections 1 and 2 (m/s),
ρ_G = gas density (assumed constant) (kg/m^3),

and the pressure difference between sections 0 and 2 may be calculated using the momentum equation for steady flow (noting that $A_1 = A_2$).

$$P_0 - P_2 = \rho_G U_G^2 \left[1 - \left(\frac{A_1}{A_0}\right)\right]. \qquad [3]$$

Addition of [2] and [3] gives

$$\Delta P = \frac{1}{2}\rho_G U_G^2 \left[1 - \left(\frac{A_1}{A_0}\right)\right]^2. \qquad [4]$$

The derivation of [4] requires the assumption that there is no separation of the gas flow before the crest of the wave.

The force balance in the vertical direction is obtained by applying the momentum equation to control volume A between sections 1 and 2 (see figure 10). It is assumed that the momentum flux through sections 1 and 2 is the same, that is that the gas and liquid velocity distributions are the same at sections 1 and 2. The weight of the gas phase is neglected, so that for steady flow the forces arising from differences in pressure between sections 1 and 2 must be balanced only by the weight of the liquid wave and the integrated wall shear stress, giving

$$\Delta P A = \rho_L W g - 2\pi D h \tau_w, \qquad [5]$$

where A = total cross-sectional area of tube ($=0.25\pi D^2$ m^2),
h = wave height (m),
W = volume of liquid in the wave (m^3),
τ_w = wall shear stress (N/m^2),

and

$$W = \pi h^2 \left(\frac{\pi D}{2} - \frac{4h}{3} \right). \quad [6]$$

A second equation connecting the wave height to the gas velocity may be obtained by postulating that the wave is in horizontal equilibrium when the flooding conditions are reached. This has been previously suggested by Ueda & Suzuki (1978) who justified the assumption with the observation that any increase in the wave amplitude would cause the gas pressure over the wave to fall and hence cause unstable growth of the wave.

The horizontal equilibrium of the wave is governed by the competing effects of surface tension forces and forces arising from differences in pressure between the liquid and gas sides of the wave. The following problems prevent a simple horizontal resolution to obtain a force balance.

1. The actual wave profile is not semicircular, and therefore the surface tension force will act at some unknown angle to the horizontal.
2. The pressure on both the gas and liquid sides of the wave varies in a complicated way between P_1 and P_2. However, the average pressure difference between the liquid and gas sides of the wave can reasonably be expected to be proportional to the total pressure drop ΔP.
3. In small diameter tubes capillary effects become important. Wallis & Makkenchery (1974) have described a tendency for the surface tension forces to "pull the liquid film into a bridge across the gas core" in small tubes.

Problems (1) and (2) may be accounted for by an unknown constant of proportionality ζ which will be determined empirically. Horizontal resolution results in the following equation, which is similar to an equation used by Ueda & Suzuki (1978):

$$\zeta\sigma = h\Delta P. \quad [7]$$

Elimination of ΔP between [5] and [7] gives

$$\frac{\zeta\sigma A}{h} = \rho_L W g - 2\pi D h \tau_w. \quad [8]$$

The wall shear stress τ_w is assumed to be unaffected by the wave, and is given by the equation

$$\tau_w = \frac{1}{2} f_w \rho_l U_l^2 \quad [9]$$

and therefore [9] becomes

$$\frac{\zeta\sigma A}{h} = \rho_L W g - \pi D h f_w \rho_l U_l^2, \quad [10]$$

where f_w = wall friction factor (−),
U_L = liquid average velocity (m/s),
ρ_L = liquid density (kg/m^3),
σ = surface tension (N/m).

The gas and liquid superficial velocities are given by the equations

$$V_G \simeq U_G, \qquad [11]$$

and

$$V_L = \left(\frac{A - A_L}{A}\right) U_L \simeq \left(\frac{4\delta}{D}\right) U_L, \qquad [12]$$

where V_G = gas superficial velocity (m/s)
V_L = liquid superficial velocity (m/s)
δ = mean falling film thickness (m).

Substitution of equations [6], [11] and [12] into [10] provides an equation which relates the wave height at flooding to the liquid superficial velocity.

$$\frac{\zeta\sigma D^2}{4h^3} - \rho_l g\left(\frac{\pi D}{2} - \frac{4h}{3}\right) + \frac{f_w \rho_l D}{h}\left(\frac{D}{4\delta}\right)^2 V_l^2 = 0. \qquad [13]$$

Before [13] can be solved to find the wave height at flooding it is necessary to be able to calculate the thickness of the falling liquid film δ. Bankoff & Lee (1985) have discussed the calculation of the mean film thickness of a falling liquid film in both laminar and turbulent flow. They compared experimental film thickness data with the predictions of two equations and found good agreement. For laminar flow the equation used was that of Nusselt (1916) which may be written

$$\delta^* = 0.908\,(\mathrm{Re}_{sl})^{0.333}, \qquad [14]$$

where Re_{sL} = liquid superficial Reynolds number ($\mathrm{Re}_{sL} = \rho_l V_l D/\mu_l$),
μ_L = liquid dynamic viscosity (Ns/m^2),
and δ^* = dimensionless film thickness defined by

$$\delta^* = \delta\left[\frac{g\rho_l(\rho_l - \rho_g)}{\mu_l^2}\right]^{1/3}. \qquad [15]$$

For turbulent flow Bankoff & Lee (1985) recommended the use of an equation due Belkin *et al.* (1959)

$$\delta^* = 0.135\,(\mathrm{Re}_{sl})^{0.583}. \qquad [16]$$

Equations [14] and [16] are used to determine the mean liquid film thickness. The transition between the two equations is taken to occur at $\mathrm{Re}_{sl} = 2064$ (where the two equations predict the same liquid film thickness). Equations [14] and [16] were developed for the calculation of the liquid film thickness in the absence of a countercurrent gas flow, the presence of which would be expected to thicken the film. However, the results of Dukler *et al.* (1984) indicate that [14] gives good prediction of the film thickness even for gas velocities approaching the flooding gas velocity.

After calculation of the liquid film thickness, [13] may be solved to calculate the wave amplitude at which flooding would be expected to occur. Equation [13] involves the fourth power of h but has only one solution in the range $0 \leq h \leq D/2$, and this solution may easily be found by interval halving. The flooding gas velocity may now be calculated by substitution of the critical wave height into [5] or [7].

If the foregoing analysis is applied for the flow in an annulus the following equations enable calculation of the critical wave height and the flooding gas velocity.

$$\frac{\zeta\sigma[D_a^2 - D_r^2]}{4h^3} - \rho_L g\left(\frac{\pi D_r}{2} + \frac{4h}{3}\right) + \frac{f_w \rho_L D_r}{h}\left(\frac{A}{A - A_1}\right)^2 V_L^2 = 0, \quad [17]$$

$$\sigma\zeta = h\Delta P, \quad [18]$$

where $A = 0.25\pi(D_a^2 - D_r^2)$,
$A_0 = 0.25\pi\{D_a^2 - [D_r + 2(\delta + h)]^2\}$,
$A_L = 0.25\pi[D_a^2 - (D_r + 2\delta)^2]$,
D_a = diameter of outer tube (m),
D_r = diameter of central rod (m),

and ΔP is calculated from [4].

For low pressure systems where $\rho_L \gg \rho_G$ it is interesting to note that if the wave amplitude h and the mean falling film thickness δ are considered small in comparison with the tube diameter D, and if the wall shear stress is neglected, [5] and [6] may be rearranged to give

$$V_G^* = \left(\frac{\pi}{4}\right)^{1/2}, \quad [19]$$

where V_G^* = gas dimensionless superficial velocity at flooding,
and $V_G^* = V_G \rho_G^{1/2}\,[gD(\rho_L - \rho_G)]^{-1/2}$

5.1. *Validity of the analysis*

During the course of the foregoing analysis it has been necessary to make many simplifying assumptions, and these have been stated at appropriate points. It is useful here to consider the validity of these simplifying assumptions, and where possible to consider the possibility of using less simple alternatives. The main assumptions are considered individually below.

5.1.1. *The wave profile.* The profile of the stationary liquid wave formed on the surface of the liquid film has been assumed to be semicircular. Analysis of figure 9 shows that this assumption is not strictly valid, but that the chosen wave profile is no less reasonable than the possible alternatives (for example square, triangular or sinusoidal), and also that the length of the stationary wave is approximately twice its height. Furthermore, it is easy to show that the weight of the liquid wave of given height and length is not particularly sensitive to the chosen profile.

5.1.2. *Calculation of the pressure drop.* The change in the gas pressure between sections 1 and 2 (see figure 10) has been calculated by the application of Bernoulli's equation (section 1 to section 0) and the momentum equation (section 0 to section 2). A turbulent flow computer program has been used to obtain pressure drop predictions for the assumed wave profile and for a typical gas velocity and wave height. The predictions thus obtained have been compared with those of [4], and reasonable agreement has been obtained. This indicates that the assumptions made in the derivation of [4] are valid for the flow conditions here.

5.1.3. *The vertical force balance.* The force balance in the vertical direction has been obtained by applying the momentum equation to control volume A in figure 10. Two major assumptions were necessary:

1. That the liquid momentum flux entering the control volume is identical to the liquid momentum flux leaving the control volume. This assumption is not valid, because the

velocity profile in the liquid film will be affected by the presence of the liquid wave, and also because some of the liquid film will move into the wave to increase its size and cause its instability. However, only two extreme situations can be analysed—that none or all of the liquid momentum flux is destroyed. Of these the chosen situation would seem more reasonable, and further it may be shown that the liquid momentum flux is small compared to the gas momentum flux.

2. That the gas momentum flux entering the control volume is the same as the gas momentum flux leaving the control volume. This is obviously an approximation because the gas velocity profile will require a finite axial length to settle down after the disturbance cause by the liquid wave. This could be to some extent accounted for in [5] by extending the control volume further downstream (referring to the gas) of the wave to allow the gas flow to settle down. The integrated wall shear stress term in [5] would increase in proportion to the length of the control volume, but this effect would be offset by the need to introduce a term to allow for the weight of liquid in the falling film. The net effect would be small.

An alternative to [5] would be to use a turbulent flow computer program to calculate the total force applied by the gas to the liquid wave. Such an analysis would require an accurate knowledge of the wave profile and also of the interfacial shear stress, neither of which is available.

The assumptions made in the foregoing analysis may therefore only be partially justified. The most likely source of error is that in a real situation there will be a change in the gas momentum flux between sections 1 and 2 in figure 10. This will have a significant effect on the validity of [5] but, as has been outlined above, alternative approaches are not available. Finally, it is relevant to note that in view of the complexity of flooding problem the assumptions are thought to be reasonable, and certainly no less reasonable than those made in other simple treatments of flooding.

6. COMPARISON WITH EXPERIMENT

The equations resulting from the foregoing analysis may be used to predict the height of the liquid wave and the gas velocity at flooding for flow in annuli, in terms of the profile factor ζ. The predictions of the analysis may therefore be compared with the experimental results of section 3 above, and the appropriate value of ζ selected. Calculation shows that the liquid superficial Reynolds numbers vary between approximately 500 and 4000, and in view of the turbulence of the gas phase the liquid film flow close to the flooding point would be expected to be transitional. The wall friction factor f_w was therefore given the value of $f_w = 0.01$ (see for example Miller 1978).

In figure 8 the predictions of [17] and [18] are compared with the experimental flooding gas velocities for flow in an annulus. The value of ζ was 0.5. Figure 8 shows good agreement between the experimental and calculated flooding velocities. In figure 11 the predicted wave height at flooding is plotted as a function of the water flowrate. Figure 11 also includes experimental wave heights measured from the high-speed cine films of flooding in an annulus. Again, good agreement is obtained.

In figure 12 the predictions of [7] and [13] are compared with flooding gas velocities for flow in a tube calculated from the experimental results presented by Whalley & McQuillan (1985). The results plotted are for a tube length of 0.5 m (so that the tube length is similar to the rod length used in the annulus experiments), and the value of ζ was 0.5 (the value which enabled good agreement to be achieved in figure 8). It may be seen from figure 12 that the agreement between the experimental and theoretical flooding velocities is remarkably good, and further that the effect of changes in gas density on the flooding gas velocity is well predicted.

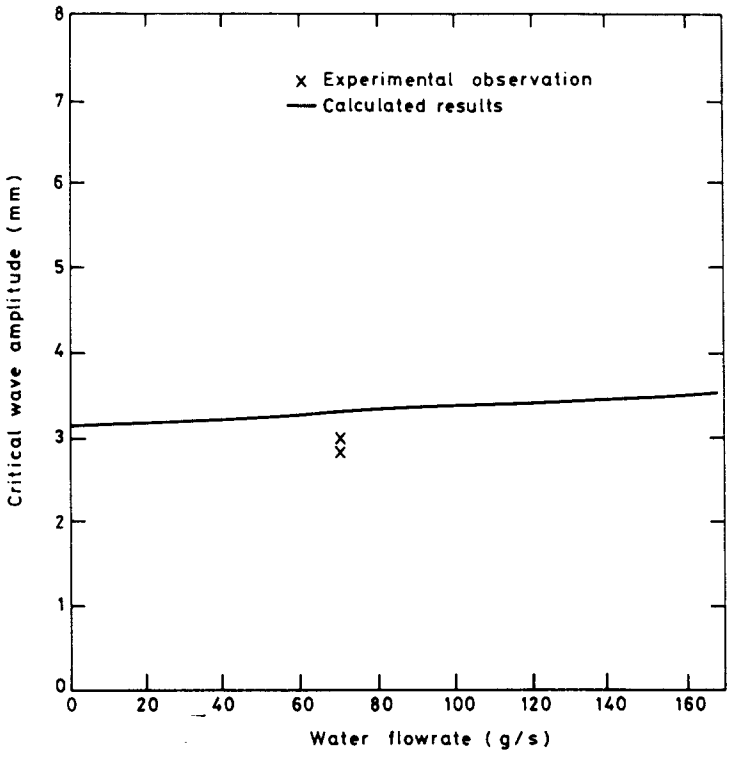

Figure 11. Experimental and predicted critical wave heights for flooding in the annulus.

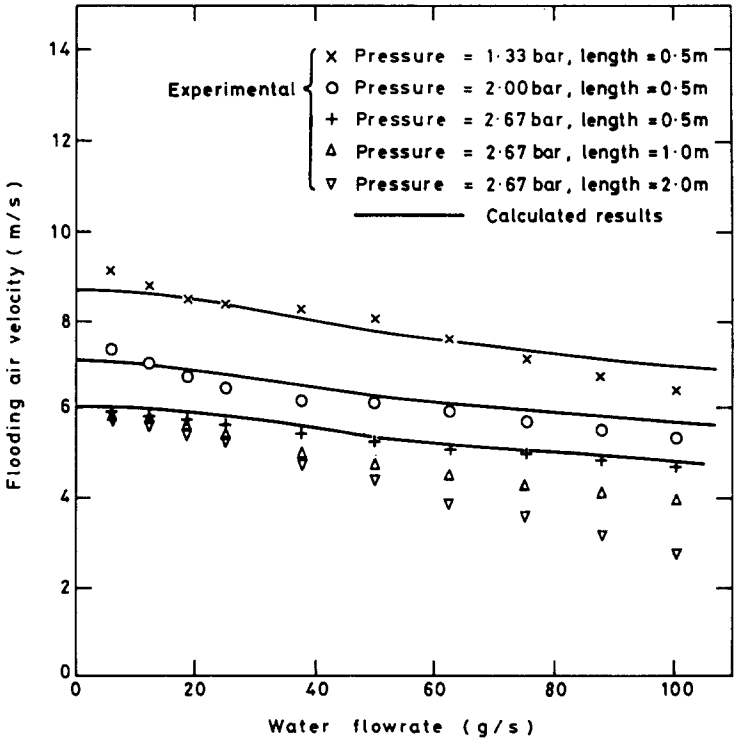

Figure 12. Experimental and predicted flooding velocities for flow in a tube (Whalley & McQuillan, 1984a).

McQuillan & Whalley (1985) have compared the predictions of a number of flooding theories and empirical flooding correlations with a large collection of flooding data. The present theory is in better agreement with the data than the other flooding theories tested, but is not as good as the best of the empirical correlations.

The results of Whalley & McQuillan (1985) have shown that, in the absence of localised disturbances at the liquid exit, the flooding gas velocity for a given liquid velocity increases as the length of tube between the liquid inlet and outlet decreases. This effect can be seen in figure 12 where for one pressure (2.67 bar) experimental results are given for three different tube lengths, 0.5 m, 1.0 m and 2.0 m. The flooding model described above is based on the hypothesis that a liquid wave of the critical size exists somewhere in the tube when the gas velocity reaches the flooding gas velocity. In order to make allowance for the effects of tube length it would be necessary to have an equation which gives the wave height as a function of the distance through which the wave has fallen, the gas and liquid flowrates and the fluid properties.

7. CONCLUSIONS

This paper has described two experiments in which the formation and motion of the flooding disturbance has been observed with the aid of high-speed cine photography. The observations have provided information about the mechanism of flooding, and suggested the basis of a simple theoretical treatment of flooding. The resulting equations are in good agreement with experimental data obtained here for an annulus and by Whalley & McQuillan (1985) for a tube.

Acknowledgement—This work was supported by the United Kingdom Atomic Energy Authority (A.E.R.E. Harwell).

NOMENCLATURE

- A tube cross sectional area, m^2
- D diameter, m
- f friction factor
- g acceleration of gravity, 9.81 m/s^2
- h wave amplitude, m
- P pressure, N/m^2
- Re Reynolds number
- ΔP pressure change, N/m^2
- U average velocity, m/s
- V superficial velocity, m/s
- W volume of liquid in wave, m^3
- δ mean falling film thickness, m
- ζ profile factor
- μ dynamic viscosity, Ns/m^2
- ρ density, kg/m^3
- σ surface tension, N/m
- τ shear stress, N/m^2

Subscripts

- a annulus
- G gas
- L liquid
- r central rod

s superficial
w wall
0 section 0
1 section 1
2 section 2

Superscript
* nondimensionalised quantity as indicated

REFERENCES

BANKOFF, S. G. & LEE, S. C. 1985 A critical review of the flooding literature. To be published in *Multiphase Science and Technology* **2,** by Hemisphere Publishing, New York.

BELKIN, H. H., MACLEOD, A. A., MONRAD, C. C. & ROTHFUS, R. R. 1959 Turbulent liquid flow down vertical walls. *AIChE J.* **5,** 245–248.

DUKLER, A. E., SMITH, L. & CHOPRA, A. 1984 Flooding and upwards film flow in tubes. I. Experimental studies. *Int. J. Multiphase Flow* **10,** 585–597.

HEWITT, G. F. & WHALLEY, P. B. 1980 Advanced optical instrumentation methods. *Int. J. Multiphase Flow* **6,** 139–156.

MCQUILLAN, K. W. & WHALLEY, P. B. 1985 Comparison between flooding correlations and experimental flooding data. Accepted for publication in *Chem. Eng. Science.*

MILLER, D. S. 1978 Internal flow systems. Published by BHRA Fluids Engineering.

NUSSELT, W. 1916 Surface condensation of water vapour. *Z.Ver.D.Ing* **60**(27), 541–546; **60**(26), 569–575.

RICHTER, H. J. 1981 Flooding in tubes and annuli. *Int. J. Multiphase Flow* **7,** 647–658.

SHEARER, C. J. & DAVIDSON, J. F. 1965 The investigation of a standing wave due to gas blowing upwards over a liquid film; Its relation to flooding in wetted wall columns. *J. Fluid Mech.* **22,** 321–336.

UEDA, T. & SUZUKI, S. 1978 Behaviour of liquid films and flooding in counter-current two-phase flow. Part 2. Flow in annuli and rod bundles. *Int. J. Multiphase Flow* **4,** 157–170.

WALLIS, G. B. & MAKKENCHERY, S. 1974 The hanging film phenomenon in vertical annular two-phase flow. *J. Fluids. Eng.* **96**(3), 297–298.

WHALLEY, P. B. & MCQUILLAN, K. W. 1984 The use of axial view photography to observe flooding in gas-liquid two-phase flow. AERE-M3380.

WHALLEY, P. B. & MCQUILLAN, K. W. 1985 Flooding in two-phase flow: The effect of tube length and artificial wave injection. *Physiochemical Hydrodynamics* **6,** 3–21.